Article:
Peralta-Arriaga, S.L., Fernández-Terán, R.J., Shipp, J.D. et al. (2024) Photophysics of Fe-Fe hydrogenase mimic complexes for hydrogen evolution. Journal of Organometallic Chemistry, 1004. 122940. ISSN: 0022-328X

https://doi.org/10.1016/j.jorganchem.2023.122940

Journal of Organometallic Chemistry 1004 (2024) 122940

Contents lists available at ScienceDirect

Journal of Organometallic Chemistry

journal homepage: www.elsevier.com/locate/jorganchem

Photophysics of Fe-Fe hydrogenase mimic complexes for hydrogen evolution

Samantha L. Peralta-Arriaga, Ricardo J. Fernández-Terán, James D. Shipp, Catherine E. Royle, Dimitri Chekulaev, Michael J. Morris, Julia A. Weinstein *

Department of Chemistry, University of Sheffield, Sheffield S3 7HF, United Kingdom

ARTICLE INFO

Keywords:
Proton reduction
Hydrogenase mimics
Ultrafast infrared spectroscopy
Photochemistry
Photocatalysis
Electrochemistry

ABSTRACT

The photophysical and electrochemical properties of the diiron hydrogenase mimic complex, $[Fe_2(dpet)(CO)_6]$ (dpet = 1,2-diphenylethene-1,2-dithiol) have been studied using a combination of spectroscopic and electrochemical techniques including cyclic voltammetry, infrared spectroelectrochemistry (IR-SEC), ultrafast transient absorption (TA) spectroscopy and time-resolved infrared spectroscopy (TRIR), with the data interpretation aided by density functional theory (DFT). The complex is a viable catalyst for electrochemical hydrogen evolution, as shown by its electrochemical reversibility and significant increase in the catalytic current upon addition of trifluoroacetic acid (TFA). IR-SEC was used to identify the first and second reduction products, where formation of a bridging μ-CO species was observed. The ultrafast spectroscopy data show that CO loss is only a minor excited state relaxation pathway, unlike other previously reported [FeFe] catalysts, in agreement with steady-state photolysis. The excited state lifetime obtained for this complex (135 ps in DCM and 237 ps in MeCN) is insufficient for $[Fe_2(dpet)(CO)_6]$ to function as a photocatalyst on its own. However, the photostability of the complex opens up an opportunity for its future use in conjunction with a photosensitiser in photochemical hydrogen evolution.

1. Introduction

There is a clear need to develop new renewable technologies to produce fuels that help us to move towards a more sustainable world. Hydrogen (H_2) is considered one of the most promising combustible alternatives to the hydrocarbon fuels in current use [1,2]. As dihydrogen production is energy-intensive, ideally, the energy required would be provided by sunlight. Therefore, the development of catalytic systems capable of solar-driven dihydrogen formation is highly desirable [3]. Since the seminal work by Honda and Fujishima in the 1970s, who used UV light and TiO_2 to split water into hydrogen and oxygen, a plethora of artificial photocatalytic systems aimed at proton reduction or water splitting have been reported [3–6].

Whilst the goal would be photochemical water "splitting" [7–9], an intermediate target is to focus on the reduction part of the process—namely, on using visible light to drive catalytic production of dihydrogen from protons [10]. Accordingly, the optimisation and development of efficient catalysts based on earth-abundant materials such as iron is an active area of research [11,12]. In nature, enzymes called hydrogenases are used by various organisms to reduce protons in dark reactions [13]. The active site in hydrogenases [14,15], commonly called the "H-cluster", typically includes a binuclear centre with a general formula $[M_2(S\hat{}S)(L)_6]$ where M_2 = [Fe-Fe], [Fe-Ni] or [Fe-N], ligated to a bridging dithiolate ligand (S^S), and to non-protic CN^- or CO ligands (L) [15–21]. The hydrogenase mimics that are considered the most efficient catalysts for proton reduction are based on the [FeFe] motif [22–26]. These complexes have been shown to reduce protons with turnover frequencies around $10^3\ s^{-1}$. Additionally, [FeFe] catalysts are less sensitive to inhibition by oxygen and carbon monoxide and operate under lower overpotentials in water in comparison to [NiFe] hydrogenases [15]. Many [FeFe] mimics have been synthesised, bearing different types of aromatic bridging ligands e.g., 1,2-benzenedithiolate (bdt); alkylic bridging ligands such as 1,2-ethanedithiolate (edt), propane-dithiolate (pdt), or azodithiolate (adt) ligands [21,27,28]. The other ligands can also be modified, where one or more of the CO groups is replaced CN^- or phosphines [19,27,29–40]. Catalysts with aromatic bridges are preferred, as they can undergo reversible two-electron reduction at potentials of approximately –1.3 V (vs Fc^+/Fc^0),

* Corresponding author.
E-mail address: Julia.Weinstein@Sheffield.ac.uk (J.A. Weinstein).

https://doi.org/10.1016/j.jorganchem.2023.122940
Received 27 June 2023; Received in revised form 28 September 2023; Accepted 1 November 2023
Available online 2 November 2023

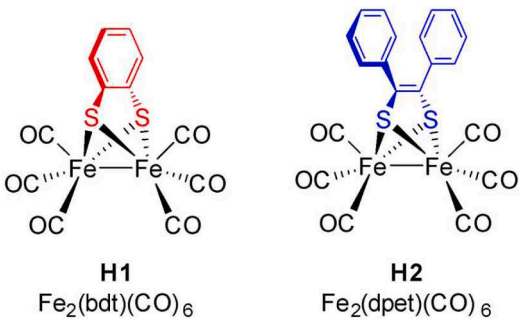

Scheme 1. Structures of **H1,** $Fe_2(bdt)(CO)_6$ (*left*); and **H2,** $Fe_2(dpet)(CO)_6$ (*right*).

considerably less negative than those with the aliphatic (e.g., pdt) bridged ligands, which undergo an irreversible reduction at –1.67 V (vs Fc^+/Fc^0) [41–43]. For the case of alkylenedithiolate species, the reduction is usually irreversible, and the reduced species cannot be detected by cyclic voltammetry due to fast decomposition of the reduction product. This is thought to occur mainly through CO loss [10, 44–47]. Interestingly, doubly-reduced species have been detected at the first reduction potential during electrolysis of $[Fe_2(bdt)(CO)_6]$ in MeCN by IR-SEC [10,48,49] due to the product of one-electron reduction being reduced at less negative potentials than the neutral, parent compound. It was shown that increasing the electron-withdrawing character of the bridge in the arenedithiolate complexes $[Fe_2(\mu\text{-}S_2Ar)(CO)_6]$ (Ar = benzene, toluene, 3,6-dichlorobenzene and quinoxaline) led to lower electron density of the diiron core, resulting in a decrease in the electrocatalytic proton reduction overpotential [33,34,48,50,51].

Several examples of photochemical hydrogen evolution using [FeFe] catalysts alongside photosensitisers have been reported previously [52–54]. The development of a catalytic system for solar-driven hydrogen production using [FeFe] mimics—ideally, as the light-absorbing units themselves—as proton reduction catalysts requires a detailed understanding of the excited state dynamics of these complexes. Such understanding can also inform the design of new complexes which can be activated by visible light [40,55], either directly, or following electron transfer from a photosensitiser. Since the catalysts contain strong IR-absorbers—namely the CO and CN ligands, time-resolved infrared spectroscopy (TRIR) is a method of choice to study their excited state dynamics [56–62].

A recent TRIR study of $[Fe_2(pdt)(CO)_6]$, which contains an aliphatic dithiolate bridge, showed that the excited state undergoes CO loss, alongside other relaxation processes on 7–10 ps timescales, followed by vibrational cooling on the 30–60 ps timescale, while the solvent adduct persists beyond the 1-ns time window [55,63]. TRIR studies of $[Fe_2(bdt)(CO)_6]$, containing an aromatic dithiolate bridge in *n*-heptane, carbon tetrachloride, chloroform, methylene chloride, tetrahydrofuran, and toluene, after 400 nm excitation, revealed that the excited state decays on a timescale shorter than 5 ps, whilst the nature of electronic excited state(s) is not clear [64].

This work presents the study of a hydrogenase mimic complex, $[Fe_2(dpet)(CO)_6]$ (**H2**), where dpet = 1,2-diphenyl-1,2-dithioethane, Scheme 1. The aromatic dpet ligand was selected as it potentially allows for reversible two-electron reduction of the catalyst (vs. irreversible reductions of the complexes with aliphatic dithiolate bridges) due to an increase on the size of the π system respect to that of the commonly used bdt ligand in $[Fe_2(bdt)(CO)_6]$ (**H1**). The **H2** complex was studied by a combination of electrochemical, IR-SEC, and ultrafast TA and TRIR spectroscopy methods, supported by (time-dependant-)density functional theory [(TD-)DFT] calculations. The aim was to characterise the redox behaviour and the excited state dynamics of the new hydrogenase mimic and to further our understanding of the fundamental excited state dynamics of [FeFe] catalysts in general, which could allow for their application in photochemical hydrogen evolution.

2. Experimental section

2.1. Synthesis and characterization of Fe-Fe complexes

$[Fe_2(dpet)(CO)_6]$ (**H2**) and $[Fe_2(bdt)(CO)_6]$ (**H1**) were prepared according to literature methods [66]. **H1** and **H2** were characterized by NMR spectroscopy, FT-IR spectroscopy, and mass spectrometry. Analytical data for **H2** are given in the SI and correspond to those reported previously [66].

Fourier-transform infrared spectroscopy (FT-IR) was carried out with a PerkinElmer One Spectrometer, using a liquid transmission CaF_2 cell (OMNI Cell®), with a 2 cm^{-1} resolution.

The ^1H and ^{13}C NMR spectra of the synthesized complexes were recorded on a Bruker Avance 400 spectrometer. Deuterated solvents were purchased from Sigma-Aldrich and were of spectroscopic grade. All chemical shifts are reported in parts per million (ppm), with ^1H NMR spectra being calibrated relative to the residual solvent signal.

Mass-spectra were analysed in a Waters LTC Mass Spectrometry equipment with Atmospheric Pressure Chemical Ionisation (APCI) for non-polar molecules in the mass range 100–3000 Da.

The redox potentials were determined by cyclic voltammetry using a Metrohm Autolab PGSTAT100 potentiostat, in a three-electrode cell. The reference, working, and counter electrodes were Ag/AgCl (0.1 mol L^{-1}), glassy-carbon and platinum wire, respectively. All measurements were carried out in dry MeCN with $[^nBu_4N][PF_6]$ (0.5 mol L^{-1}, purified by recrystallization from EtOH) as supporting electrolyte. Dry MeCN was obtained from the University of Sheffield solvent purification service. The redox potentials were calculated against the Fc^+/Fc° couple as an internal reference. The linear dependence of the current vs the square root of the scan rate for individual redox couples was used to check whether the processes were reversible and diffusion-controlled.

UV–Vis absorption spectra were recorded on a Cary 50 UV–Vis spectrometer using quartz cuvettes of 1 cm path length. The photostability of the complexes was evaluated using a continuous wave 405 nm LED diode (Thorlabs, 1 mW cm^{-2}) as the irradiation source in MeCN and dichloromethane (DCM) using a gas-tight 1 cm quartz cell to avoid any changes in concentration due to solvent evaporation. Spectra were collected every 5 min up to a total time of 10 h, using an in-house automated Arduino controller.

The spectroscopic changes upon electrochemical reduction in anhydrous MeCN were investigated by IR-SEC using the same potentiostat and FT-IR spectrometer described above, in an optically transparent thin-layer electrochemical (OTTLE) cell, consisting of two CaF_2 optical windows, a Pt minigrid counter- and working electrodes, and an Ag wire as pseudo-reference electrode [67].

Femtosecond Transient Absorption (TA) spectroscopy was performed at the Lord Porter Laser Laboratory, University of Sheffield. A Ti: Sapphire regenerative amplifier (Spitfire ACE PA-40, Spectra-Physics) provided 800 nm pulses (40 fs FWHM, 10 kHz, 1.2 mJ). 400 nm pulses for excitation were generated by doubling a portion of the 800 nm output in a β-barium borate crystal within a commercially available doubler/tripler (TimePlate, Photop Technologies). White light supercontinuum probe pulses in the range 340–790 nm, were generated by tightly focusing ca. 1 μJ of the 800 nm output on a CaF_2 crystal (continuously displaced to avoid damage). Detection was achieved using a commercial transient absorption spectrometer (Helios, Ultrafast Systems) using a 2048-pixel CMOS sensor for the UV–Vis spectral range. The relative polarisation of the pump and probe pulses was set to the magic angle of 54.7° for anisotropy-free measurements. Samples were held in 2 mm pathlength quartz cells and were stirred during experiments. The optical density at the excitation wavelength was kept at approximately 0.5. The optical density across the probe range was kept below 1.0. Excitation energies were kept below 2 μJ.

Time-resolved infrared spectroscopy (TRIR) was performed at the

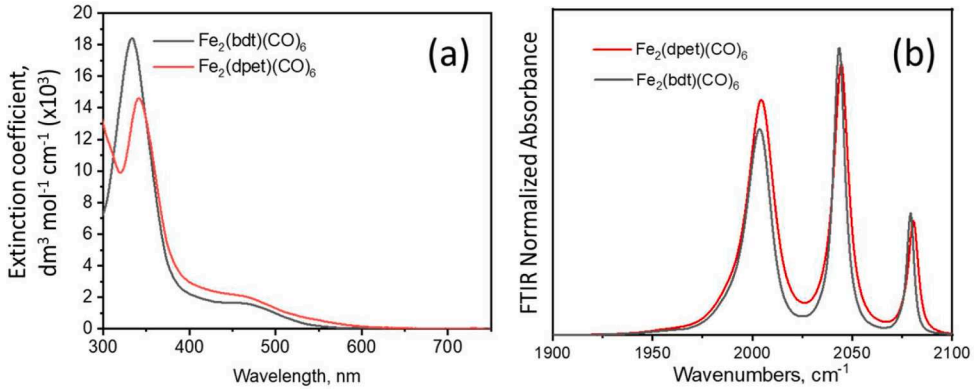

Fig. 1. UV Vis (a) and FTIR (b) absorption spectra of **H1** [$Fe_2(bdt)(CO)_6$] (black) and **H2** [$Fe_2(dpet)(CO)_6$] (red) recorded in a 50 μM solution in MeCN at room temperature. (For interpretation of the references to colour in this figure legend, the reader is referred to the web version of this article.).

Lord Porter Ultrafast Laser Spectroscopy Laboratory, University of Sheffield using the same laser source as described above. 410 nm pulses for sample excitation were generated with a commercially available optical parametric amplifier (TOPAS Prime, Light Conversion). Broadband IR pulses were produced by an automated commercially available optical parametric amplifier equipped with a difference frequency mixing stage (TOPAS Prime, Light Conversion). A Ge filter was used to remove the residual signal and idler. The mid-IR light was divided into probe and reference beams with a 50/50 Ge beam splitter. Samples were prepared in 650 μm pathlength liquid cells (Harrick Scientific) equipped with 2 mm CaF_2 windows. Samples were flowed with a peristaltic pump and continuously rastered during measurements to minimise photodecomposition. The optical density across the probe region was kept below 1.0. Detection was achieved with two liquid-nitrogen-cooled 128-pixel HgCdTe (MCT) arrays (FPAS, Infrared Systems Development), coupled with automated spectrometers (iHR 320, HORIBA). The relative polarisation of the UV and mid-IR beams was set to the magic angle of 54.7° for anisotropy-free measurements.

Density functional theory (DFT) calculations were performed in Gaussian 16, Rev. C.01 [68], using the B3LYP functional and a split basis set consisting of the 6–311 G (d,p) basis set for all light atoms and the LANL2DZ basis set and ECP for the Fe atoms. Solvent effects were accounted for by the Gaussian implementation of the IEF-PCM model for MeCN and DCM. For each complex, the ground state (S_0), the lowest triplet excited state (T_1), as well as the corresponding singly and doubly reduced species were calculated in both MeCN and DCM and optimised under tight convergence criteria. Convergence to a minimum was confirmed by frequency calculations, which did not yield any negative frequencies. The frequencies obtained from these calculations were scaled by 0.973 to better match the experimentally obtained frequencies and convoluted with a Lorentzian function (FWHM 8 cm^{-1}) to generate the calculated absolute and difference spectra in all cases. Time-dependent density functional theory (TD-DFT) calculations were performed under identical conditions as described above, considering the lowest 30 singlet and 30 triplet states. The calculated UV–Vis absorption spectra were generated by convolution with a Gaussian function with a uniform FWHM of 1850 cm^{-1} and were shifted to higher energies to better match the experiment by 0.35 eV (**H1**) and 0.25 eV (**H2**), respectively. Charge density difference isosurfaces were generated from the Gaussian outputs and formatted checkpoint files with the help of the MultiWfn program (v. 3.7) [69].

Fragment-based population analysis and transition density decomposition analysis, were performed in a similar manner as in a recent publication of ours [70], using the TheoDORE program (v3.0) [71], with the inbuilt transition density matrix analysis modules [72,73]. Calculations considering only the lowest 30 singlet states of all complexes were performed, including the options pop = full iop(9/40 = 3) for compatibility. The energies and oscillator strengths obtained from these calculations were identical to those that included the triplet states. The TheoDORE program internally uses the CCLIB library (v1.7.2) [74] to parse the output of the Gaussian calculations [69].

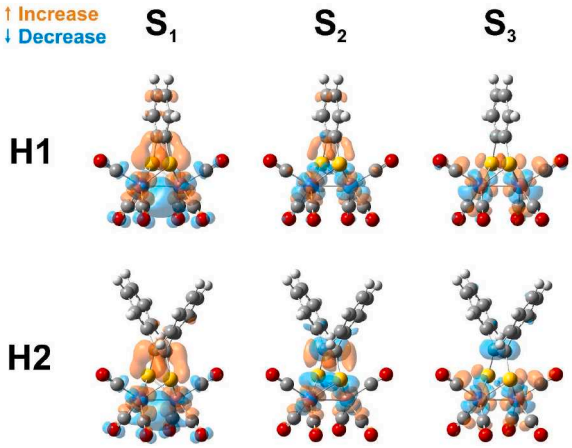

Fig. 2. Charge density difference isosurfaces plotted for the lowest three excited singlet states for complexes **H1** and **H2**. Isosurfaces plotted at $|\Delta\rho|$ = 0.002 a.u.

3. Results

3.1. UV visible and FTIR spectroscopy

The UV–Vis absorption spectra of both **H1** and **H2** (Fig. 1a) shows an intense band in the range of 300–375 nm (λ_{max} 333 nm) for **H1** and at 320–400 nm (λ_{max} 340 nm) for **H2** [60]. The absorption band at lower energies (ca. 460 nm, ε 1600 dm^3 cm^{-1} mol^{-1}) has been assigned to a metal/metal-to-ligand charge transfer (MLCT) transition from the σ Fe−Fe to the σ* S-ligand orbitals [49,65,75,76] on the basis of TD-DFT calculations (Fig. 2 and **Figure S1**).

The FT-IR spectra of **H1** and **H2** in the 1900–2100 cm^{-1} region (Fig. 1b) contain three prominent absorption bands, attributed to group stretching vibrations of the Fe/CO ligands ν(CO). These bands are similar for both complexes, with a minimal (1 cm^{-1}) small shift of ν(CO) to higher frequencies for **H2** (2080, 2043, 2004 cm^{-1}) compared to **H1**. The FTIR spectra of **H1** and **H2** are similar to that reported in hexane for [$Fe_2(pdt)(CO)_6$] with an aliphatic dithiolate ligand, which has transitions at 2075, 2035, 2006, and 1991 cm^{-1} and a weaker transition at 1982 cm^{-1} [63].

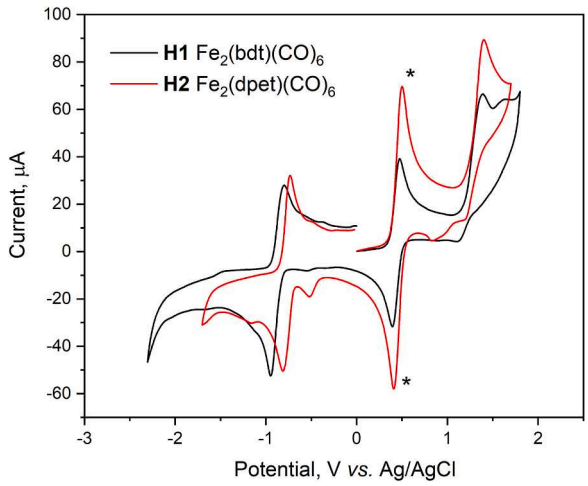

Fig. 3. Cyclic voltammogram of a 1 mM solution of **H1** and **H2** in 0.1 M [^{n}Bu$_4$][PF$_6$] in dry MeCN, at a scan rate of 100 mV s^{-1} under N$_2$ atmosphere, in presence of Fc/Fc$^+$ (*).

3.2. Electrochemical characterization

The cyclic voltammograms for the solutions of complexes **H2** and **H1** in MeCN show a reversible two-electron reduction process with half-wave potentials ($E_{1/2}$) of –1.21 V for **H2** and –1.46 V for **H1** vs Fc/Fc$^+$ (Fig. 3). The first reduction process in both complexes is electrochemically reversible, as evident from a linear dependence of the peak current vs. the square root of the scan rate ($v^{1/2}$), according to the Randles–Ševčík equation (Table S1, Fig. S2 in the ESI). The $E_{1/2}$ value for **H1** agrees with previously reported data for this complex [10]. Two one-electron reduction processes occur, whereas the second reduction takes place at less negative potential, in an electron transfer → chemical reaction → electron transfer (ECE) process, yielding an overall two-electron redox wave, consistent with previous reports [10,77,78].

3.3. Current enhancement in the presence of a proton source

Current enhancement experiments were performed to determine whether **H2** can act as a proton reduction catalyst [79]. Cyclic voltammograms of a 1 mM solution of **H2** in MeCN were recorded in the presence of 1–20 mM of TFA, with the data for **H1** recorded for comparison. The addition of a strong acid such as TFA, leads to an appearance of a reduction peak at ca. –2.3 V in solutions of both **H1** and **H2** (Fig. 4 and additional data in Figs. S3–S5 in the SI). The plot of i_{cat}/i_p as a function of concentration of TFA for **H2** is given in the SI (Fig. S5).

The reduction processes showed a linear increase in the catalytic current upon addition of TFA up to 10 mM. From the data recorded at 100 mV s^{-1}, the efficiency was estimated from the ratio of the cathodic current with/without acid, i_{cat}/i_p (Fig. S3-S5). At a TFA concentration of 10 mM, the ratio of i_{cat}/i_p was 11 for **H1** and 16 for **H2**, indicating that under these conditions, the new mimic **H2** is similar, or slightly more efficient than **H1**, for which the reported value of TOF was 7×10^4 s^{-1} in dilute sulfuric acid [32,80–83]. One can thus estimate the corresponding TOF of **H2** to be in the order of 1×10^5 s^{-1}, obtained by multiplying the TOF of **H1** by the ratio of the i_{cat}/i_p values for **H1** and **H2**, as a coarse approximation.

The observed hysteresis in the cyclic voltammograms at high TFA concentrations (>10 mM) may be linked to the aforementioned ECE reduction mechanism, where the chemical reaction product diffuses back toward the electrode during the reverse scan, causing an increase in current relative to the forward scan. It is possible that at high TFA concentrations there is a sufficient build-up of protonated catalyst in the proximity of the electrode to cause such an effect. The shift in the apparent reduction potential with the increase in [TFA] may also be due to acid concentration affecting the catalytic overpotential. Some contribution from a direct proton reduction cannot be excluded, although its contribution would be larger in **H1** (where the shift in

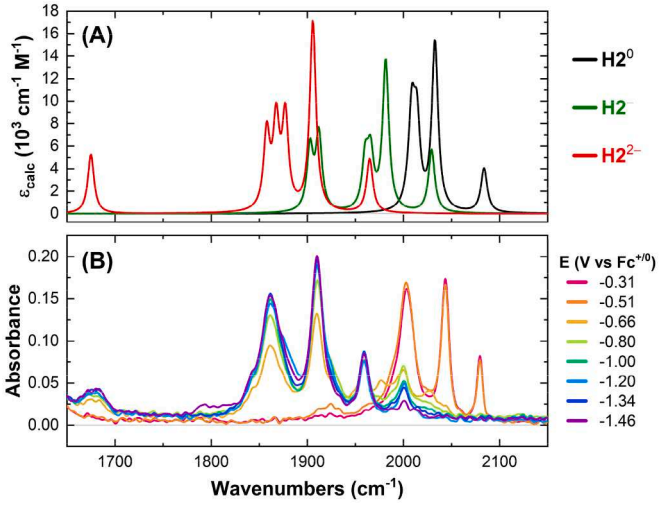

Fig. 5. (A) Calculated IR spectra of the different redox species associated with the reduction of **H2** in MeCN. Calculated frequencies were scaled by 0.973 to better match the experimental values. (B) Experimental IR-SEC spectra of **H2** in MeCN.

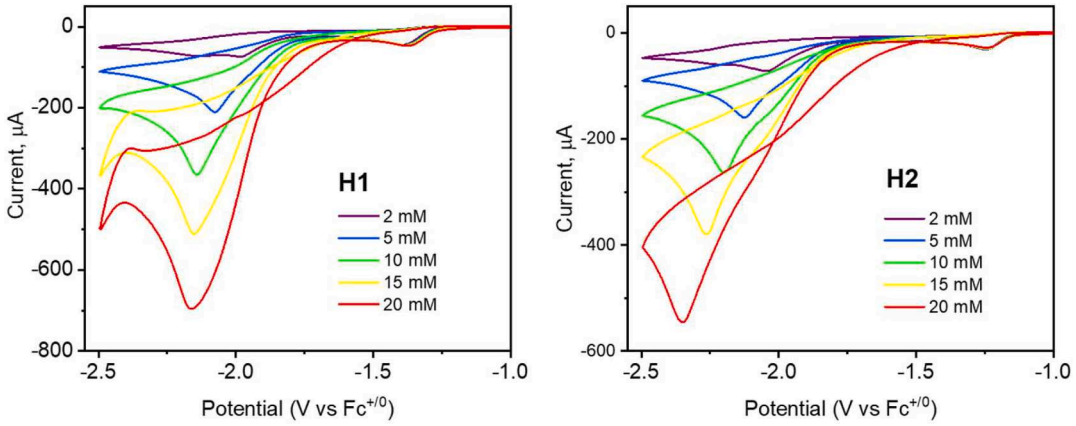

Fig. 4. Cyclic voltammetry of solutions of **H1** (left) and **H2** (right) at increasing concentration of TFA (2 mM to 20 mM) in 0.1 M [nBu$_4$][PF$_6$] in dry MeCN at a scan rate of 100 mV s^{-1} under N$_2$ atmosphere.

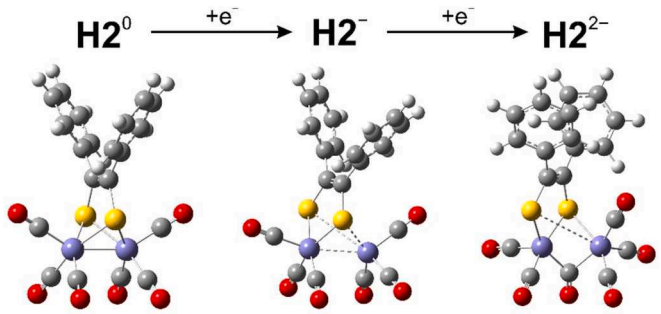

Fig. 6. DFT-optimised structures of the sequential reductions of complex **H2**.

overpotential is 140 mV vs. 40 mV in **H2**).

3.4. FTIR spectroelectrochemistry (IR-SEC)

To elucidate the changes in the structure in response to the reduction process, the Fe-Fe complexes were analysed by infrared spectroelectrochemistry. Fig. 5 illustrates changes in the IR spectra of **H2** in the course of reduction: the bands at 2080, 2043 and 2003 cm^{-1} that correspond to the group stretching vibrations of the $Fe_2(CO)_6$ moiety of the $Fe_2(dpet)(CO)_6$ complex in its neutral form disappear, and new bands appear at 1960, 1909, and 1860 cm^{-1}, corresponding to the doubly reduced form, $[Fe_2(dpet)(CO)_6]^{2-}$. The original FTIR spectrum has been fully restored upon re-oxidation of the Fe°Fe° form, indicating chemical reversibility of the two-electron reduction process in **H2** under the experimental conditions used (Fig. S6). This result agreed with the results obtained for **H1,** $Fe_2(bdt)(CO)_6$, whereas upon first reduction the three parent absorption bands of ν(CO) at 2080, 2043 and 2004 cm^{-1} decrease in intensity, whilst new bands appear at lower energies 1964, 1913 and 1862 cm^{-1} corresponding to the ν(CO) of the doubly reduced complex, $[Fe_2(bdt)(CO)_6]^{2-}$ [84].

The results obtained from IR-SEC (Fig. 5a) are supported by DFT calculations (Fig. 5b) which show an excellent match between the experimental and the calculated spectra for the doubly-reduced species. The data also hint at a small amount of the singly reduced species being produced at less negative potentials in the forward scan (compare e.g. a small peak at 1975 cm^{-1} in Fig. 5**b** at the applied potential –0.66 V, and the spectrum calculated for $\mathbf{H2}^-$ in Fig. 5**a**, green trace).

With the aid of DFT calculations, we propose a mechanism for the reduction processes happening in **H2**. Our results agree with previous reports whereas it is suggested that the first reduction leads to a distortion of the molecule due to the reduction of one of the Fe-atoms in the "H-cluster" accompanied by reduction in FeFe bond order, and an increase of the FeFe and Fe-S distances for the reduced Fe-centre. The second reduction, more thermodynamically favourable than the first one, leads to breaking of the Fe–Fe bond, and the rearrangement of one of the CO ligands into a bridging mode between the two iron centres (Fig. 6). The calculated and experimental values are similar, as can be seen from the similarity in the spectra presented in Fig. 5, which supports this mechanistic proposal.

3.5. Ultrafast photoinduced dynamics of the hydrogenase mimic

Catalysts need to be able to form an excited state with sufficiently long lifetime to initiate a bimolecular reaction of the reduction of H^+ to H_2. To investigate the excited state dynamics of **H2** including the nature of the excited state(s) and their lifetimes, we have employed pump–probe visible transient absorption (TA) and time-resolved infrared (TRIR) spectroscopy following electronic excitation with narrowband 400–410 nm, ca. 40 fs laser pulses. The TA spectra were recorded in the range from ca. 430 nm to ca. 740 nm (this range is limited by the scattering of the 400 nm excitation pulse, and the 800 nm fundamental wavelengths of the laser used, see Experimental for details). The TRIR data were recorded in the range 1850–2200 cm^{-1}, to detect ν(CO) modes. The experimental data are shown in Fig. 7, and their modelling is shown in Fig. 8. The characters of the involved excited state are shown in Fig. 2, in the context of the discussion of the TRIR spectra. The time constants extracted from the data analysis are summarised in Table 1, with the resulting schematic energy level diagram shown in Fig. 10. The excited state dynamics was investigated in acetonitrile (MeCN) and in dichloromethane (DCM).

3.5.1. Excited state dynamics of *H2* in acetonitrile

The TA spectra of **H2** in MeCN at early time delays after the excitation are comprised of two broad positive signals due to excited state absorption (ESA) bands at ca. 460, 560 nm (Fig. 7b). To model the decay dynamics of the transient spectrum satisfactorily required four first-order decay components (assuming a sequential model with A → B → C → D) in the global analysis. The time constants extracted were 4.0 ± 0.1 ps, 24.6 ± 0.7 ps, and 135 ± 6 ps, and "infinity". The spectra of the first 3 components (Fig. 8b) are similar, and likely to belong to the state

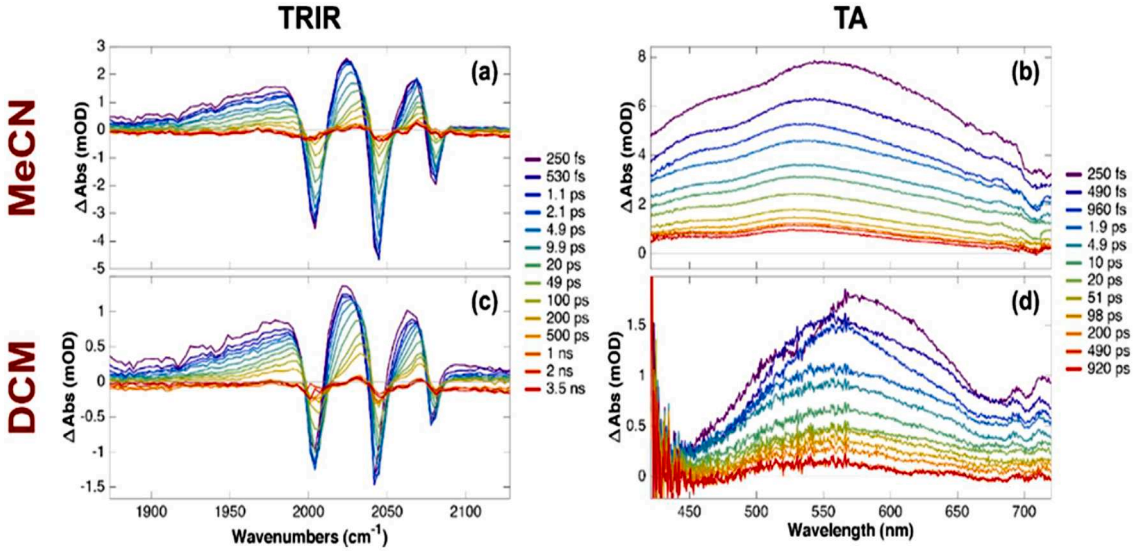

Fig. 7. Time-resolved infrared spectra (TRIR) (*left column*) and electronic transient absorption spectra (TA, *right column*), of **H2** in MeCN (*a-b*) and DCM (*c-d*). TRIR experiments were performed with 410 nm excitation, TA experiments with 400 nm excitation, ca. 40 fs pulses.

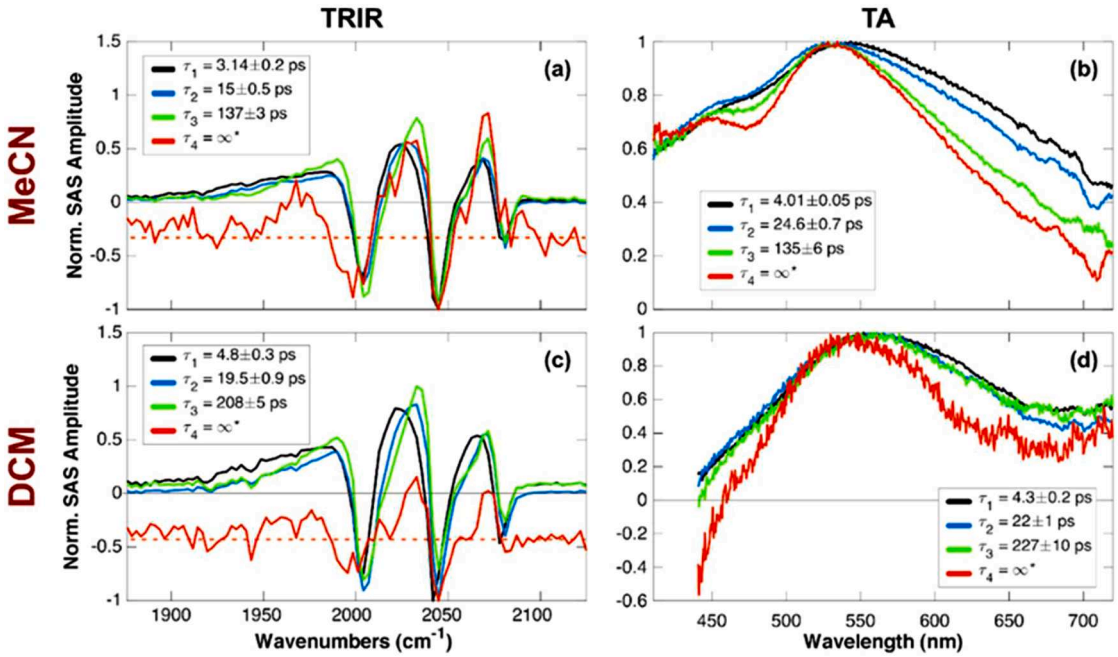

Fig. 8. Analysis of the data presented in Fig. 7. Normalised species-associated spectra derived from target analysis of the TRIR (left column) and TA (right column) datasets for **H2** in MeCN (a-b) and DCM (c-d). *The dotted orange lines in (a) and (c) indicate the presence of a small amount (1 %) of a long-lived component–it is offset for clarity. Please note that the species-associated spectra are normalised, to compare spectral shape–this representation does not reflect the relative amplitude of each component.

Table 1
Summary of time constants derived from target analysis of the time-resolved spectra of **H2**, following 400–410 nm, ~40 fs excitation in different solvents, using a sequential four-state model.

Solvent	Time constant (ps)	TRIR	TA
MeCN	τ_1	3.1 ± 0.2	4.01 ± 0.05
	τ_2	15.0 ± 0.5	24.6 ± 0.7
	τ_3	137 ± 3	135 ± 6
DCM	τ_1	4.8 ± 0.3	4.3 ± 0.2
	τ_2	19.5 ± 0.9	23 ± 1
	τ_3	208 ± 5	227 ± 10

(s) of the same origin. There is a gradual narrowing of the absorption bands, and the low-energy shoulder becomes more pronounced with time. The final time constant—accounting for ca. 1 % of the initially excited molecules—was fixed to an infinitely long lifetime to account for residual signal present beyond the timescale of the experiment (a few ns). This component is attributed to a permanent photoproduct resulting from sample photolysis during the measurements, as shown in the following section.

The TRIR spectra of **H2** in MeCN (Fig. 7a) exhibit three negative bands corresponding to ground state bleaches (GSB) of the γ group vibrations of the $Fe_2(CO)_6$ moiety (2004, 2044, and 2080 cm^{-1}), where each GSB is paired with an excited state transient signal at 1990 (very broad, overlap of multiple transitions), 2024, and 2068 cm^{-1}. The long-

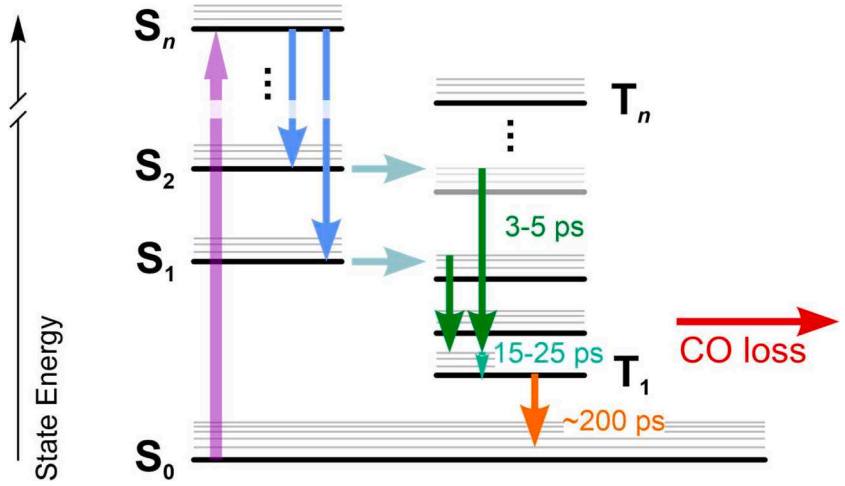

Fig. 9. Schematic energy level diagram highlighting the observed processes: after photoexcitation to a manifold of singlet states, the complex undergoes internal conversion and intersystem crossing to the triplet manifold, within the instrument response of our equipment. This is followed by internal conversion in the triplet manifold (τ_1), vibrational cooling (τ_2), and decay to the ground state (τ_3), see Table 1 for the values of τ_1- τ_3. Along the way, a dissociative potential energy surface is intercepted, and CO loss takes place, albeit with a very low efficiency (for **H2** in acetonitrile, we estimate it as ca. 1 %). It is however unclear at which point the complex does evolve CO.

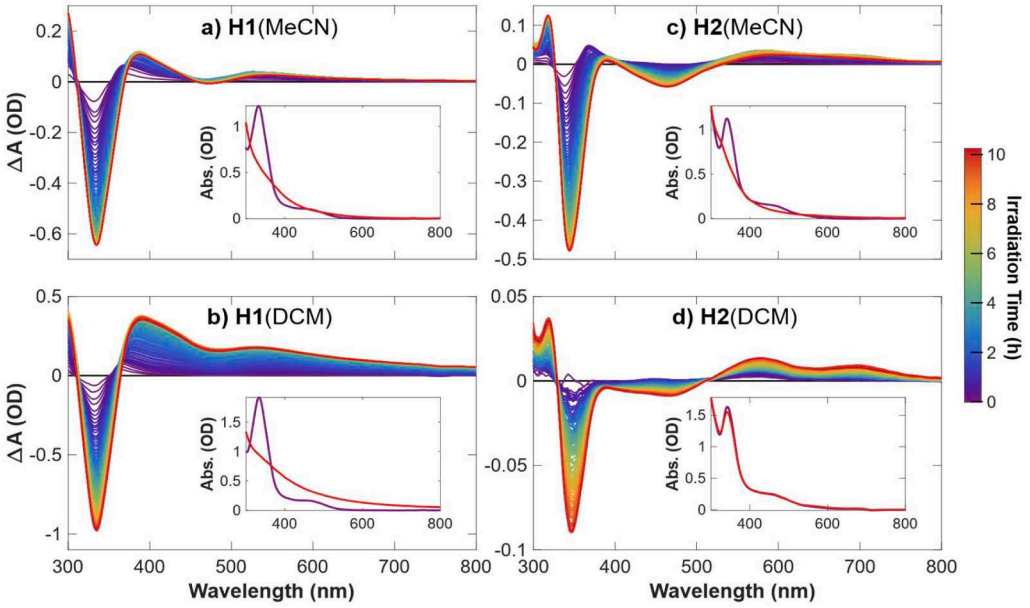

Fig. 10. UV–Vis absorption spectra of a 0.1 mM solution of $[Fe_2(bdt)(CO)_6]$ (**H1**) and $[Fe_2(dpet)(CO)_6]$ (**H2**) as a function of irradiation time in different solvents: in MeCN (a, c) and DCM (b, d), respectively. Irradiation was performed with 405 nm light at 1 mW cm^{-2} over 10 h. Insets show first and last spectra (purple and red, respectively). (For interpretation of the references to colour in this figure legend, the reader is referred to the web version of this article.)

lived product of photolysis has absorptions at 1968, 2033, and 2069 cm^{-1}.

For comparison, $Fe(CO)_5$ [85] has ν(CO) in hexane at 2000 and 2023 cm^{-1}—at lower frequencies than **H2**—reflecting the effect of the Fe–Fe bond (as well as e^--donating S-ligands) on the electron density of the Fe centre, and consequently, on the Fe→CO (d-π*) back-donation. The decrease in vibrational frequency upon electronic excitation is thus consistent with the shift in electron density from the Fe–Fe bonding orbital to the S-ligands, which in turn increases electron density on the Fe centre and increases back-donation. A slight shift of the ν(CO) excited state transient bands to higher frequencies on the timescale of several tens of picoseconds is consistent with vibrational cooling of the electronic excited states in transition metal carbonyls [55].

Similarly to the TA data, the TRIR signals undergo multi-exponential decay best described with a sequential four-component model, with the time constants 3.1 ± 0.2 ps, 15.0 ± 0.5 ps, 137 ± 3 ps, and "infinity" (Table 1) being very similar to those obtained from TA data. The species-associated IR spectra obtained from the sequential model can be used to propose a mechanism for the excited state relaxation of these complexes. The excited state formed immediately after excitation is assigned to a ^{1}MM/MLCT state (Figs. S8-S11 in the SI), based on the assignment of the absorption spectra. This state is too short-lived to be detected in the TRIR experiments (where the IRF is at least 200 fs). The initial spectra (<10 ps) observed in the TRIR experiment closely match those calculated for the T_1 state by DFT (Fig. S7 in the SI), which has a primarily ^{3}MLCT character. Therefore, it is likely that **H2** undergoes intersystem crossing from the singlet to triplet MLCT manifolds on the ultrafast timescale, within the instrument response period. We note that some Fe complexes are reported to form quintet states by ISC, but (TD-)DFT calculations indicate that this is unlikely for **H2**.

The profile of the species associated spectra (SAS) extracted from the TRIR spectra for $\tau_1 = 3.1$ ps and $\tau_2 = 15.0$ ps are very similar, and show no ground state recovery. Therefore, we believe both kinetic components correspond to excited states of very similar character. τ_1 can be tentatively assigned to a relaxation within the triplet manifold. The next component (τ_2) is associated with a shift in the ESA bands in the TRIR spectra and can be attributed to vibrational cooling of the excited state.

The 15-ps timescale of this process is similar to the timescale of vibrational relaxation previously observed by both TRIR and transient two-dimensional IR spectroscopy [63]. The third kinetic component (ca. 200 ps) is accompanied by the reduction in the ground state bleach, and is assigned to the decay to the ground state. However, a minor channel forming a long-lived photolysis product is also observed, as the bleach does not recover fully, and a small residual transient spectrum (which has a distinct band at 1970 cm^{-1} that is absent from the spectra of the other three short-lived excited states) persists beyond the timescale of the experiment: this product is attributed to photoinduced dissociation of a CO ligand.

The solvent dependence of the excited state dynamics was assessed by comparing the relaxation rates in MeCN and DCM (Fig. 7c, TRIR; and Fig. 7d, TA of **H2** in DCM, Table 1). The spectral shape in both solvents, and the overall dynamics, are similar, but the ESA bands observed by TA are somewhat narrower in the less polar DCM, which can be anticipated. The faster decay of the excited state in MeCN could be due to the rapid solvation of the vacant site at the Fe-centre formed by CO loss. The simplified photophysical diagram summarising these results is shown in Fig. 9.

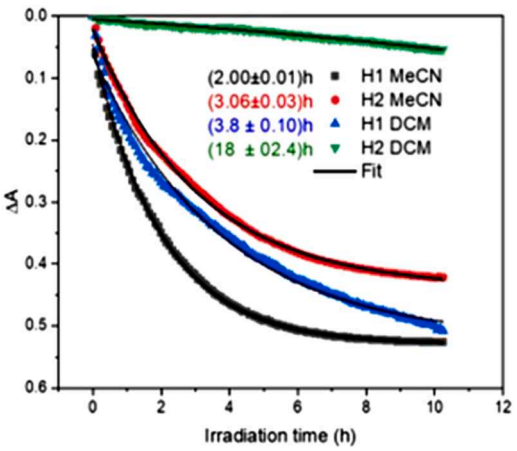

Fig. 11. The photodegradation kinetics of each sample based on the data in Fig. 10. The data show that **H2** in DCM is far more stable in comparison to the other samples with a degradation rate constant higher than 10 h^{-1}.

3.6. Photolysis and photostability of H1 and H2

The photostability of **H2** and **H1** in DCM and MeCN under 405 nm irradiation (1 mW cm^{-2}) was monitored by UV–Vis spectroscopy (Figs. 10 and 11). For **H1** in both solvents, and **H2** in MeCN, there was a noticeable reduction of the band at 333 nm within the first 5 min of irradiation. This band corresponds to the Fe-CO transitions (as described above), suggesting a loss of CO—in line with the ultrafast experiments. At the same time, new bands centred around 460 nm and 700 nm appeared and grow in intensity until ca. 90 min of irradiation. These bands later decay due to photoproduct decomposition. The new absorption band (at ca. 700 nm) could be attributed to the formation of a photo-reduced species $[Fe_2(dpet)(CO)_6]^{2-}$.

The results from the ultrafast spectroscopic measurements are in line with the lower photostability exhibited by both complexes upon photoirradiation in MeCN (Fig. 10**a, c**) versus the slower photodegradation observed in DCM. It is noteworthy that **H2** degrades ca. 6 times slower than the reference complex (**H1**) in DCM, whilst the kinetics of photodegradation are very similar in MeCN for both complexes (Fig. 11).

4. Conclusions

In summary, we have investigated the photophysical behaviour of a [FeFe]-hydrogenase mimic complex, $[Fe_2(dpet)(CO)_6]$ (**H2**) and of $[Fe_2(bdt)(CO)_6]$ (**H1**) as a comparison, using electrochemical and IR-Spectroelectrochemical methods, and ultrafast electronic (transient absorption) and time-resolved infrared (TRIR) laser spectroscopic techniques. The dpet-derivative (**H2**) has a more conjugated and somewhat more flexible Ph—C(S)═C(S)—Ph bridging unit vs. that of its benzenedithiol counterpart (**H1**). The reduction potential of **H2** is ca. 100 mV less negative than that of **H1**, making it more suitable to enact proton reduction. The suitability of **H2** for proton reduction was confirmed by current enhancement in presence of a proton source (TFA) in acetonitrile: **H2** is slightly more efficient in comparison to **H1** with a somewhat higher catalytic current ratio (i_{cat}/i_p = 16 vs 11) under the same conditions, suggesting TOF in the order of 10^5 s^{-1}. Importantly, IR spectroelectrochemistry (IR-SEC) has confirmed chemical reversibility of the reduction of **H2** under inert atmosphere. The mechanism of reduction, including independent reduction of the first Fe-centre, followed by a second reduction leading to a bridging CO ligand, was proposed based on IR-SEC and supported by DFT calculations. With the view of future development for photocatalytic proton reduction, the photostability of **H2** was established in dichloromethane, and was surprisingly higher than in acetonitrile confirmed by the photolysis results. Ultrafast time-resolved UV–Vis and IR spectroscopies were used to determine the mechanism of excited state relaxation of **H2** in MeCN and DCM on fs–ps timescales. We show that 400–410 nm excitation results in the formation of a short-lived ^{1}MLCT state. A four-state sequential model with three kinetic components were used to model the relaxation dynamics, tentatively including intersystem crossing in the charge-transfer manifold, vibrational cooling, and the ground state recovery. The surprisingly good photostability of the [FeFe] complex in acetonitrile, and its ability to act as an efficient electrocatalyst indicate its potential to work in tandem with a photosensitiser in a light-driven catalytic system.

Declaration of Competing Interest

The authors declare that they have no known competing financial interests or personal relationships that could have appeared to influence the work reported in this paper.

Data availability

Data will be made available on request.

Acknowledgements

We thank the EPSRC UK and its Capital Equipment award to the Lord Porter Laser Laboratory, and the University of Sheffield for support. The Mexican Research Council and the Energy Secretary CONACYT-SENER (Scholarship Grant number 472714, to S. L. P.-A.), the Grantham Centre for Sustainable Futures at the University of Sheffield (J. D. S.), and the STFC (C. E. R.) are acknowledged for their support of respective PhD studentships. R. F.-T. thanks the Swiss National Science Foundation for their financial support through an Early Postdoc. Mobility grant (P2ZHP2 199422), and J. A. W. is grateful to the Leverhulme Trust for the award of a Senior Research Fellowship.

Supplementary materials

Supplementary material associated with this article can be found, in the online version, at doi:10.1016/j.jorganchem.2023.122940.

References

[1] D. Streich, Y. Astuti, M. Orlandi, L. Schwartz, R. Lomoth, L. Hammarström, S. Ott, High-turnover photochemical hydrogen production catalyzed by a model complex of the [FeFe]-hydrogenase active site, Chem. A Eur. J. 16 (1) (2010) 60–63, https://doi.org/10.1002/chem.200902489.
[2] K.R. Brereton, A.G. Bonn, A.J.M. Miller, Molecular photoelectrocatalysts for light-driven hydrogen production, ACS Energy Lett 3 (5) (2018) 1128–1136, https://doi.org/10.1021/acsenergylett.8b00255.
[3] A. Fujishima, K. Honda, Electrochemical photolysis of water at a semiconductor electrode, Nature 238 (5358) (1972) 37–38, https://doi.org/10.1038/238037a0.
[4] K. Hashimoto, H. Irie, A. Fujishima, TiO_2 photocatalysis: a historical overview and future prospects, Jpn. J. Appl. Phys., Part 1 44 (12) (2005) 8269–8285, https://doi.org/10.1143/JJAP.44.8269.
[5] Y. Tachibana, L. Vayssieres, J.R. Durrant, Artificial photosynthesis for solar water-splitting, Nat. Photonics 6 (8) (2012) 511–518, https://doi.org/10.1038/nphoton.2012.175.
[6] A.M. Brown, L.J. Antila, M. Mirmohades, S. Pullen, S. Ott, L. Hammarström, Ultrafast electron transfer between dye and catalyst on a mesoporous NiO surface, J. Am. Chem. Soc. 138 (26) (2016) 8060–8063, https://doi.org/10.1021/jacs.6b03889.
[7] R.E. Blankenship, Early evolution of photosynthesis, Plant Physiol. 154 (2) (2010) 434–438, https://doi.org/10.1104/pp.110.161687.
[8] N. Nelson, C.F. Yocum, Structure and function of photosystems I and II, Annu. Rev. Plant Biol. 57 (2006) 521–565, https://doi.org/10.1146/annurev.arplant.57.032905.105350.
[9] D. Bhattacharya, H.S. Yoon, J.D. Hackett, Photosynthetic eukaryotes unite: endosymbiosis connects the dots, BioEssays 26 (1) (2004) 50–60, https://doi.org/10.1002/bies.10376.
[10] M. Mirmohades, S. Pullen, M. Stein, S. Maji, S. Ott, L. Hammarström, R. Lomoth, Direct observation of key catalytic intermediates in a photoinduced proton reduction cycle with a diiron carbonyl complex, J. Am. Chem. Soc. 136 (50) (2014) 17366–17369, https://doi.org/10.1021/ja5085817.
[11] M.E. Ahmed, A. Dey, Recent developments in bioinspired modelling of [NiFe]- and [FeFe]-Hydrogenases, Curr. Opin. Electrochem. 15 (2019) 155–164, https://doi.org/10.1016/j.coelec.2019.05.009.
[12] A. Meyers, E.J. Heilweil, C.J. Stromberg, Photodynamics of asymmetric Di-iron-cyano hydrogenases examined by time-resolved mid-infrared spectroscopy, J. Phys. Chem. A 125 (7) (2021) 1413–1423, https://doi.org/10.1021/acs.jpca.0c08921.
[13] C. Bagyinka, How does the [NiFe] hydrogenase enzyme work? Int. J. Hydrogen Energy 39 (32) (2014) 18521–18532, https://doi.org/10.1016/j.ijhydene.2014.07.009.
[14] W. Lubitz, H. Ogata, O. Rüdiger, E. Reijerse, Hydrogenases, Chem. Rev. (2014) 4081–4148, https://doi.org/10.1021/cr4005814.
[15] M. Frey, Hydrogenases: hydrogen-activating enzymes, Chembiochem 3 (2–3) (2002) 153–160, https://doi.org/10.1002/1439-7633(20020301)3:2/3<153::AID-CBIC153>3.0.CO;2-B.
[16] J.W. Peters, W.N. Lanzilotta, B.J. Lemon, L.C. Seefeldt, X-ray crystal structure of the Fe-only hydrogenase (CpI) from *Clostridium pasteurianum* to 1.8 angstrom resolution, Science 282 (5395) (1998) 1853–1858, https://doi.org/10.1126/science.282.5395.1853.
[17] A. Silakov, B. Wenk, E. Reijerse, W. Lubitz, ^{14}NHYSCORE investigation of the H-cluster of [FeFe] hydrogenase: evidence for a nitrogen in the dithiol bridge, Phys. Chem. Chem. Phys. 11 (31) (2009) 6553–6554, https://doi.org/10.1039/B905841A.
[18] M. Sensi, C. Baffert, C. Greco, G. Caserta, C. Gauquelin, L. Saujet, M. Fontecave, S. Roy, V. Artero, P. Soucaille, I. Meynial-Salles, H. Bottin, L. De Gioia, V. Fourmond, C. Léger, L. Bertini, Reactivity of the excited states of the H-cluster of FeFe hydrogenases, J. Am. Chem. Soc. 138 (41) (2016) 13612–13618, https://doi.org/10.1021/jacs.6b06603.

[19] W. Thornley, S.A. Wirick, M. Riedel-Topper, N.J. Deyonker, T.E. Bitterwolf, C. J. Stromberg, E.J. Heilweil, Photodynamics of [FeFe]-hydrogenase model compounds with bidentate heterocyclic ligands, J. Phys. Chem. B 123 (33) (2019) 7137–7148, https://doi.org/10.1021/acs.jpcb.9b04675.

[20] Ö.F. Erdem, L. Schwartz, M. Stein, A. Silakov, S. Kaur-Ghumaan, P. Huang, S. Ott, E.J. Reijerse, W. Lubitz, A model of the [FeFe] hydrogenase active site with a biologically relevant azadithiolate bridge: a spectroscopic and theoretical investigation, Angewandte Chemie - Int. Ed. 50 (6) (2011) 1439–1443, https://doi.org/10.1002/anie.201006244.

[21] G. Berggren, A. Adamska, C. Lambertz, T.R. Simmons, J. Esselborn, M. Atta, S. Gambarelli, J.M. Mouesca, E. Reijerse, W. Lubitz, T. Happe, V. Artero, M. Fontecave, Biomimetic assembly and activation of [FeFe]-hydrogenases, Nature 499 (2013) 66–69, https://doi.org/10.1038/nature12239.

[22] F. Arrigoni, G. Zampella, L. De Gioia, C. Greco, L. Bertini, The photochemistry of $Fe_2(S_2C_3H_6)(CO)_6(\mu\text{-}CO)$ and its oxidized form, two simple [FeFe]-hydrogenase CO-inhibited models. A DFT and TDDFT investigation, Inorganics 9 (2) (2021) 16, https://doi.org/10.3390/inorganics9020016.

[23] M. Natarajan, N. Kumar, M. Joshi, M. Stein, S. Kaur-Ghumaan, Mechanism of Diiron hydrogenase complexes controlled by nature of bridging dithiolate ligand, ChemistryOpen 11 (1) (2022), https://doi.org/10.1002/open.202100238.

[24] G. Hogarth, An unexpected leading role for $[Fe_2(CO)_6(\mu\text{-}Pdt)]$ in our understanding of [FeFe]-H_2ases and the search for clean hydrogen production, Coord. Chem. Rev. 490 (2023), 215174, https://doi.org/10.1016/j.ccr.2023.215174.

[25] G.R.F. Orton, S. Ghosh, L. Alker, J.C. Sarker, D. Pugh, M.G. Richmond, F. Hartl, G. Hogarth, Biomimics of [FeFe]-hydrogenases incorporating redox-active ligands: synthesis, redox properties and spectroelectrochemistry of diiron-dithiolate complexes with ferrocenyl-diphosphines as Fe_4S_4 surrogates, Dalton Trans. 51 (25) (2022) 9748–9769, https://doi.org/10.1039/D2DT00419D.

[26] T. Agarwal, S. Kaur-Ghumaan, Macrocyclic butterfly iron cluster complexes: electrochemical investigations, J. Chem. Sci. 132 (2020) 125, https://doi.org/10.1007/s12039-020-01830-0.

[27] T.R. Simmons, G. Berggren, M. Bacchi, M. Fontecave, V. Artero, Mimicking hydrogenases: from biomimetics to artificial enzymes, Coord. Chem. Rev. (2014) 127–150, https://doi.org/10.1016/j.ccr.2013.12.018.

[28] M.E. Ahmed, A. Nayek, A. Križan, N. Coutard, A. Morozan, S. Ghosh Dey, R. Lomoth, L. Hammarström, V. Artero, A. Dey, A bidirectional bioinspired [FeFe]-hydrogenase model, J. Am. Chem. Soc. 144 (8) (2022) 3614–3625, https://doi.org/10.1021/jacs.1c12605.

[29] J. Amaro-Gahete, M.V. Pavliuk, H. Tian, D. Esquivel, F.J. Romero-Salguero, S. Ott, Catalytic systems mimicking the [FeFe]-hydrogenase active site for visible-light-driven hydrogen production, Coord. Chem. Rev. 448 (2021) 214172, https://doi.org/10.1016/j.ccr.2021.214172.

[30] C. Papini, C. Sommer, L. Pecqueur, D. Pramanik, S. Roy, E.J. Reijerse, F. Wittkamp, V. Artero, W. Lubitz, M. Fontecave, Bioinspired artificial [FeFe]-hydrogenase with a synthetic H-cluster, ACS Catal. 9 (5) (2019) 4495–4501, https://doi.org/10.1021/acscatal.9b00540.

[31] M. Watanabe, Y. Honda, H. Hagiwara, T. Ishihara, [FeFe]-hydrogenase and its organic molecule mimics — artificial and bioengineering application for hydrogen production, J. Photochem. Photobiol. C (2017) 1–26, https://doi.org/10.1016/j.jphotochemrev.2017.09.001.

[32] R. Becker, S. Amirjalayer, P. Li, S. Woutersen, J.N.H. Reek, An iron-iron hydrogenase mimic with appended electron reservoir for efficient proton reduction in aqueous media, Sci. Adv. 2 (1) (2016), https://doi.org/10.1126/sciadv.1501014.

[33] J.F. Capon, S. Ezzaher, F. Gloaguen, F.Y. Pétillon, P. Schollhammer, J. Talarmin, T. J. Davin, J.E. McGrady, K.W. Muir, Electrochemical and theoretical investigations of the reduction of $[Fe_2(CO)_5L\{\mu\text{-}SCH_2XCH_2S\}]$ complexes related to [FeFe] hydrogenase, New J. Chem. 31 (12) (2007) 2052–2064, https://doi.org/10.1039/b709273c.

[34] K. Charreteur, M. Kdider, J.F. Capon, F. Gloaguen, F.Y. Pétillon, P. Schollhammer, J. Talarmin, Effect of electron-withdrawing dithiolate bridge on the electron-transfer steps in diiron molecules related to [2Fe](H) subsite of the [FeFe]-hydrogenases, Inorg. Chem. 49 (5) (2010) 2496–2501, https://doi.org/10.1021/ic902401k.

[35] M.E. Ahmed, A. Dey, Recent developments in bioinspired modelling of [NiFe]- and [FeFe]-hydrogenases, Curr Op Elchem 15 (2019) 155–164, https://doi.org/10.1016/j.coelec.2019.05.009.

[36] G. Qian, H. Wang, W. Zhong, X. Liu, Electrochemical investigation into the electron transfer mechanism of a diiron hexacarbonyl complex bearing a bridging naphthalene moiety, Electrochim. Acta 163 (2015) 190–195, https://doi.org/10.1016/j.electacta.2015.02.163.

[37] H. Abul-Futouh, L.R. Almazahreh, M.K. Harb, H. Görls, M. El-Khateeb, W. Weigand, [FeFe]-hydrogenase H-cluster mimics with various $-S(CH_2)_nS-$ linker lengths (n = 2-8): A Systematic Study, Inorg Chem 56 (17) (2017) 10437–10451, https://doi.org/10.1021/acs.inorgchem.7b01398.

[38] G. Durgaprasad, R. Bolligarla, S.K. Das, Synthesis, crystal structure and electrocatalysis of 1,2-ene dithiolate bridged diiron carbonyl complexes in relevance to the active site of [FeFe]-hydrogenases, J Organomet Chem 706–707 (2012) 37–45, https://doi.org/10.1016/j.jorganchem.2012.01.021.

[39] R.C. Puthenkalathil, M. Etinski, B. Ensing, Unraveling the mechanism of biomimetic hydrogen fuel production-a first principles molecular dynamics study, Phys Chem Chem Phys 22 (19) (2020) 10447–10454, https://doi.org/10.1039/c9cp06770a.

[40] J.L. Bingaman, C.L. Kohnhorst, Van Meter, B.A. McElroy, E.A. Rakowski, B. W. Caplins, T.A. Gutowski, C.J. Stromberg, C.E. Webster, E.J. Heilweil, Time-resolved vibrational spectroscopy of [FeFe]-hydrogenase model compounds, J Phys Chem A 116 (27) (2012) 7261–7271, https://doi.org/10.1021/jp2121774.

[41] H. Abul-Futouh, A. Skabeev, D. Botteri, Y. Zagranyarski, H. Görls, W. Weigand, K. Peneva, Toward a tunable synthetic [FeFe]-hydrogenase H-cluster mimic mediated by perylene monoimide model complexes: insight into molecular structures and electrochemical characteristics, Organometallics 37 (19) (2018) 3278–3285, https://doi.org/10.1021/acs.organomet.8b00450.

[42] H. Abul-Futouh, W. Imhof, W. Weigand, L.R. Almazahreh, Electrochemical and computational insights into the reduction of $[Fe_2(CO)_6[m\text{-}(SCH_2)_2GeMe_2]]$ hydrogenase H-cluster mimic, Inorganics (Basel) 7 (50) (2019) 1–11, https://doi.org/10.3390/inorganics7040050.

[43] H. Abul-Futouh, H. Görls, W. Weigand, Electrochemical proton reduction catalyzed by $[Fe_2(CO)_6\{\mu\text{-}(TeCH_2Te)\}]$ model that mimics the structure of the active site of [FeFe]-hydrogenase, Z Anorg Allg Chem 644 (24) (2018) 1697–1701, https://doi.org/10.1002/zaac.201800070.

[44] J.F. Capon, F. Gloaguen, P. Schollhammer, J. Talarmin, Catalysis of the electrochemical H_2 evolution by Di-iron sub-site models, Coord Chem Rev 249 (2005) 1664–1676, https://doi.org/10.1016/j.ccr.2004.11.018.

[45] S. Wang, S. Pullen, V. Weippert, T. Liu, S. Ott, R. Lomoth, L. Hammarström, Direct spectroscopic detection of key intermediates and the turnover process in catalytic H_2 formation by a biomimetic diiron catalyst, Chem Eur J 25 (47) (2019) 11135–11140, https://doi.org/10.1002/chem.201902100.

[46] L. Bertini, M.E. Alberto, F. Arrigoni, J. Vertemara, P. Fantucci, M. Bruschi, G. Zampella, L. De Gioia, On the photochemistry of $Fe_2(Edt)(CO)_4(PMe_3)_2$, a [FeFe]-hydrogenase model: A DFT/TDDFT investigation, Int J Quantum Chem 118 (9) (2018), https://doi.org/10.1002/qua.25537.

[47] L. Bertini, C. Greco, P. Fantucci, L. De Gioia, TDDFT modeling of the CO-photolysis of $Fe_2(S_2C_3H_6)(CO)_6$, a model of the [FeFe]-hydrogenase catalytic site, Int J Quantum Chem 114 (13) (2014) 851–861, https://doi.org/10.1002/qua.24667.

[48] L. Schwartz, P.S. Singh, L. Eriksson, R. Lomoth, S. Ott, Tuning the electronic properties of $Fe_2(\mu\text{-}Arenedithiolate)(CO)_6\text{-}n(PMe_3)n$ (n = 0, 2) complexes related to the [Fe-Fe]-hydrogenase active site, Comptes Rendus Chimie 11 (8) (2008) 875–889, https://doi.org/10.1016/j.crci.2008.04.001.

[49] J.P.H. Oudsen, B. Venderbosch, D.J. Martin, T.J. Korstanje, J.N.H. Reek, M. Tromp, Spectroscopic and theoretical investigation of the $[Fe_2(Bdt)(CO)_6]$ hydrogenase mimic and some catalyst intermediates, Phys Chem Chem Phys 21 (27) (2019) 14638–14645, https://doi.org/10.1039/c9cp01393h.

[50] I.K. Pandey, S.M. Mobin, N. Deibel, B. Sarkar, S. Kaur-Ghumaan, Diiron benzenedithiolate complexes relevant to the [FeFe] hydrogenase active site, Eur J Inorg Chem 2015 (17) (2015) 2875–2882, https://doi.org/10.1002/ejic.201500345.

[51] I.K. Pandey, M. Natarajan, H. Faujdar, F. Hussain, M. Stein, S. Kaur-Ghumaan, Intramolecular stabilization of a catalytic [FeFe]-hydrogenase mimic investigated by experiment and theory, Dalton Trans 47 (14) (2018) 4941–4949, https://doi.org/10.1039/c7dt04837h.

[52] X. Li, M. Wang, L. Chen, X. Wang, J. Dong, L. Sun, Photocatalytic water reduction and study of the formation of Fe $^{I}Fe^{0}$ species in diiron catalyst sytems, ChemSusChem 5 (5) (2012) 913–919, https://doi.org/10.1002/cssc.201100490.

[53] W.M. Singh, T. Baine, S. Kudo, S. Tian, X.A.N. Ma, H. Zhou, N.J. Deyonker, T. C. Pham, J.C. Bollinger, D.L. Baker, B. Yan, C.E. Webster, X. Zhao, Electrocatalytic and photocatalytic hydrogen production in aqueous solution by a molecular cobalt complex, Angew Chem Int Ed 51 (24) (2012) 5941–5944, https://doi.org/10.1002/anie.201200082.

[54] S. Wang, A. Aster, M. Mirmohades, R. Lomoth, L. Hammarström, Structural and kinetic studies of intermediates of a biomimetic diiron proton-reduction catalyst, Inorg Chem 57 (2) (2018) 768–776, https://doi.org/10.1021/acs.inorgchem.7b02687.

[55] S. Kaziannis, S. Santabarbara, J.A. Wright, G.M. Greetham, M. Towrie, A. W. Parker, C.J. Pickett, N.T. Hunt, Femtosecond to microsecond photochemistry of a [FeFe]hydrogenase enzyme model compound, J Phys Chem B 114 (46) (2010) 15370–15379, https://doi.org/10.1021/jp107618n.

[56] M.V. Appleby, R.A. Cowin, I.I. Ivalo, S.L. Peralta-Arriaga, C.C. Robertson, S. Bartlett, A. Fitzpatrick, A. Dent, G. Karras, S. Diaz-Moreno, D. Chekulaev, J. A. Weinstein, Ultrafast electronic, infrared, and X-ray absorption spectroscopy study of Cu(I) phosphine diimine complexes, Faraday Discuss 244 (2023) 391–410, https://doi.org/10.1039/D3FD00027C.

[57] M.A. Lebedeva, T.W. Chamberlain, P.A. Scattergood, M. Delor, I.V. Sazanovich, E. S. Davies, M. Suyetin, E. Besley, M. Schröder, J.A. Weinstein, A.N. Khlobystov, Stabilising the lowest energy charge-separated state in a {metal Chromophore – Fullerene} assembly: a tuneable panchromatic absorbing donor–acceptor triad, Chem Sci 7 (9) (2016) 5908–5921, https://doi.org/10.1039/C5SC04271B.

[58] P. A. Eckert, K. J. Kubarych. Ultrafast Spectroscopy of Hydrogenase Enzyme Models. 2019, 237-258. https://doi.org/10.1007/978-981-13-9753-0_11.

[59] S. Kaziannis, S. Santabarbara, J.A. Wright, G.M. Greetham, M. Towrie, A. W. Parker, C.J. Pickett, N.T. Hunt, Femtosecond to microsecond photochemistry of a [FeFe]-hydrogenase enzyme model compound, J Phys Chem B 114 (46) (2010) 15370–15379, https://doi.org/10.1021/jp107618n.

[60] R. Becker, S. Amirjalayer, P. Li, S. Woutersen, J.N.H. Reek, An iron-iron hydrogenase mimic with appended electron reservoir for efficient proton reduction in aqueous media, Sci Adv 2 (1) (2016), https://doi.org/10.1126/sciadv.1501014.

[61] P.W.J.M. Frederix, K. Adamczyk, J.A. Wright, T. Tuttle, R.V. Ulijn, C.J. Pickett, N. T. Hunt, Investigation of the ultrafast dynamics occurring during unsensitized photocatalytic H_2 evolution by an [FeFe]-hydrogenase subsite analogue, Organometallics 33 (20) (2014) 5888–5896, https://doi.org/10.1021/om500521w.

[62] A.P.S. Samuel, D.T. Co, C.L. Stern, M.R. Wasielewski, Ultrafast photodriven intramolecular electron transfer from a zinc porphyrin to a readily reduced diiron hydrogenase model complex, J Am Chem Soc 132 (26) (2010) 8813–8815, https://doi.org/10.1021/ja100016v.

[63] A.I. Stewart, J.A. Wright, G.M. Greetham, S. Kaziannis, S. Santabarbara, M. Towrie, A.W. Parker, C.J. Pickett, N.T. Hunt, Determination of the photolysis products of [FeFe]hydrogenase enzyme model systems using ultrafast multidimensional infrared spectroscopy, Inorg Chem 49 (2010) 9563–9573, https://doi.org/10.1021/ic101289s.

[64] B.W. Caplins, J.P. Lomont, S.C. Nguyen, C.B. Harris, Vibrational cooling dynamics of a [FeFe]-hydrogenase mimic probed by time-resolved infrared spectroscopy, J Phys Chem A 118 (49) (2014) 11529–11540, https://doi.org/10.1021/jp510517z.

[65] R.J. DeKock, E.J. Baerends, R. Hengelmolen, The nature of the LUMO in $Fe_2(CO)_6S_2$ and the bonding in $Fe_2(CO)_6S_2^{2-}$, Organometallics 3 (2) (1984) 289–292, https://doi.org/10.1021/om00080a022.

[66] H. Adams, M.J. Morris, C.C. Robertson, H.C.I. Tunnicliffe, Synthesis of mono-and diiron dithiolene complexes as hydrogenase models by dithiolene transfer reactions, including the crystal structure of $[\{Ni(S_2C_2Ph_2)\}_6]$, Organometallics 38 (3) (2019) 665–676, https://doi.org/10.1021/acs.organomet.8b00852.

[67] S.R. Domingos, H. Luyten, F. Van Anrooij, H.J. Sanders, B.H. Bakker, W.J. Buma, F. Hartl, S. Woutersen, An optically transparent thin-layer electrochemical cell for the study of vibrational circular dichroism of chiral redox-active molecules, Rev Sci Instrum 84 (3) (2013) 2–6, https://doi.org/10.1063/1.4793722.

[68] Frisch, M.J., Trucks, G.W., Schlegel, H.B., Scuseria, G.E., Robb, M.A., Cheeseman, J.R., Scalmani, G., Barone, V., Petersson, G.A., Nakatsuji, H., Li, X., Caricato, M., Marenich, A.V., Bloino, J., Janesko, B.G., Gomperts, R., Mennucci, B., Hratchian, H.P., Ortiz, J.V., Izmaylov, A.F., Sonnenberg, J.L., Williams-Young, D., Ding, F., Lipparini, F., Egidi, F., Goings, J., Peng, B., Petrone, A., Henderson, T., Ranasinghe, D., Zakrzewski, V.G., Gao, J., Rega, N., Zheng, G., Liang, W., Hada, M., Ehara, M., Toyota, K., Fukuda, R., Hasegawa, J., Ishida, M., Nakajima, T., Honda, Y., Kitao, O., Nakai, H., Vreven, T., Throssell, K., Montgomery, J.A., Jr., Peralta, J.E., Ogliaro, F., Bearpark, M.J., Heyd, J.J., Brothers, E.N., Kudin, K.N., Staroverov, V. N., Keith, T.A., Kobayashi, R., Normand, J., Raghavachari, K., Rendell, A.P., Burant, J.C., Iyengar, S.S., Tomasi, J., Cossi, M., Millam, J.M., Klene, M., Adamo, C., Cammi, R., Ochterski, J.W., Martin, R.L., Morokuma, K., Farkas, O., Foresman, J.B., Fox, D.J. Gaussian 16, Revision C.01. Gaussian, Inc.: Wallingford CT 2019.

[69] T. Lu, F. Chen, Multiwfn: a multifunctional wavefunction analyzer, J Comput Chem 33 (5) (2012) 580–592, https://doi.org/10.1002/jcc.22885.

[70] R.J. Fernández-Terán, E. Sucre-Rosales, L. Echevarria, F.E. Hernández, Dissecting conjugation and electronic effects on the linear and non-linear optical properties of rhenium(i) carbonyl complexes, Phys Chem Chem Phys 24 (45) (2022) 28069–28079, https://doi.org/10.1039/d2cp03844g.

[71] F. Plasser, TheoDORE: a Ttoolbox for a detailed and automated analysis of electronic excited state computations, J Chem Phys 152 (8) (2020), 084108.

[72] F. Plasser, H. Lischka, Analysis of excitonic and charge transfer interactions from quantum chemical calculations, J Chem Theory Comput 8 (8) (2012) 2777–2789, https://doi.org/10.1021/ct300307c.

[73] F. Plasser, M. Wormit, A. Dreuw, New tools for the systematic analysis and visualization of electronic excitations I. formalism, J Chem Phys 141 (2) (2014), 024106, https://doi.org/10.1063/1.4885819.

[74] N.M. O'boyle, A.L. Tenderholt, K.M. Langner, Cclib: a library for package-independent computational chemistry algorithms, J Comput Chem 29 (5) (2008) 839–845, https://doi.org/10.1002/jcc.20823.

[75] I. Silaghi-Dumitrescu, T.E. Bitterwolf, R.B. King, Butterfly diradical intermediates in photochemical reactions of $Fe_2(CO)_6(\mu\text{-}S_2)$, J Am Chem Soc 128 (16) (2006) 5342–5343, https://doi.org/10.1021/ja061272q.

[76] F. Arrigoni, G. Zampella, L. De Gioia, C. Greco, L. Bertini, The photochemistry of $Fe_2(S_2C_3H_6)(CO)_6(\mu\text{-}CO)$ and its oxidized form, two simple [FeFe]-hydrogenase CO-inhibited models. A DFT and TDDFT investigation, Inorganics 9 (2) (2021) 16, https://doi.org/10.3390/inorganics9020016.

[77] M.D. Sampson, C.P. Kubiak, Manganese electrocatalysts with bulky bipyridine ligands: utilizing lewis acids to promote carbon dioxide reduction at low overpotentials, J Am Chem Soc 138 (4) (2016) 1386–1393, https://doi.org/10.1021/jacs.5b12215.

[78] M.D. Sampson, A.D. Nguyen, K.A. Grice, C.E. Moore, A.L. Rheingold, C.P. Kubiak, Manganese catalysts with bulky bipyridine ligands for the electrocatalytic reduction of carbon dioxide: eliminating dimerization and altering catalysis, J Am Chem Soc 136 (14) (2014) 5460–5471, https://doi.org/10.1021/ja501252f.

[79] S. Gao, Q. Liang, Q. Duan, D. Jiang, J. Zhao, Electrochemical proton reductions in varying acidic media by a simple synthetic hydrogenase mimic, Int J Hydrogen Energy 43 (15) (2018) 7245–7256, https://doi.org/10.1016/j.ijhydene.2018.03.010.

[80] L. James, W.Y. Fan, Proton reduction using cyclopentadienyl Fe(II) (Benzene-1,2-Dithiolato) carbonyl complexes as electrocatalysts, Int J Hydrogen Energy 45 (56) (2020) 31976–31984, https://doi.org/10.1016/j.ijhydene.2020.08.237.

[81] J.M. Savéant, E. Vianello, Potential-sweep chronoamperometry theory of kinetic currents in the case of a first order chemical reaction preceding the electron-transfer process, Electrochim. Acta 8 (12) (1963) 905–923, https://doi.org/10.1016/0013-4686(62)87046-7.

[82] A.J. Bard, L.R. Faulkner. *Electrochemical Methods : Fundamentals and Applications*, 2nd edition, Wiley, 2000.

[83] C. Costentin, G. Passard, J.-M. Savéant, Benchmarking of homogeneous electrocatalysts: overpotential, turnover frequency, limiting turnover number, J Am Chem Soc 137 (16) (2015) 5461–5467, https://doi.org/10.1021/jacs.5b00914.

[84] A. Jablonskyte, J.A. Wright, S.A. Fairhurst, L.R. Webster, C.J. Pickett, [FeFe] hydrogenase: protonation of {2Fe3S} systems and formation of super-reduced hydride states, Angew Chem Int Ed 53 (38) (2014) 10143–10146, https://doi.org/10.1002/anie.201406210.

[85] P. Portius, M. Bühl, M.W. George, F.-W. Grevels, J.J. Turner, Structure and dynamics of iron pentacarbonyl, Organometallics 38 (21) (2019) 4288–4297, https://doi.org/10.1021/acs.organomet.9b00559.